IJMMM International Journal of Minerals, Metallurgy and Materials 矿物冶金与材料学报（英文版）

Achieving oxidation protection effect for strips hot rolling via Al_2O_3 nanofluid lubrication

Jianlin Sun, Boyuan Huang, Jiaqi He, Erchao Meng, and Qianhao Chang

Cite this article as:
Jianlin Sun, Boyuan Huang, Jiaqi He, Erchao Meng, and Qianhao Chang, Achieving oxidation protection effect for strips hot rolling via Al_2O_3 nanofluid lubrication, *Int. J. Miner. Metall. Mater.*, 30(2023), No. 5, pp. 908-916. https://doi.org/10.1007/s12613-022-2493-5

Articles you may be interested in

S. M. A. Haghi, S. A. Sajjadi, and A. Babakhani, In-situ fabrication of Al(Zn)-Al_2O_3 graded composite using the aluminothermic reaction during hot pressing, *Int. J. Miner. Metall. Mater.*, 25(2018), No. 7, pp. 832-839. https://doi.org/10.1007/s12613-018-1632-5

Chen-yang Xu, Cui Wang, Ren-ze Xu, Jian-liang Zhang, and Ke-xin Jiao, Effect of Al_2O_3 on the viscosity of $CaO–SiO_2–Al_2O_3–MgO–Cr_2O_3$ slags, *Int. J. Miner. Metall. Mater.*, 28(2021), No. 5, pp. 797-803. https://doi.org/10.1007/s12613-020-2187-9

Zuo-li Li, Jun Zhao, Jia-lin Sun, Feng Gong, and Xiu-ying Ni, Reinforcing effect of graphene on the mechanical properties of Al_2O_3/TiC ceramics, *Int. J. Miner. Metall. Mater.*, 24(2017), No. 12, pp. 1403-1411. https://doi.org/10.1007/s12613-017-1533-z

Rui Wang, Yan-ping Bao, Zhi-jie Yan, Da-zhao Li, and Yan Kang, Comparison between the surface defects caused by Al_2O_3 and TiN inclusions in interstitial-free steel auto sheets, *Int. J. Miner. Metall. Mater.*, 26(2019), No. 2, pp. 178-185. https://doi.org/10.1007/s12613-019-1722-z

Liang Yang and Guo-guang Cheng, Characteristics of Al_2O_3, MnS, and TiN inclusions in the remelting process of bearing steel, *Int. J. Miner. Metall. Mater.*, 24(2017), No. 8, pp. 869-875. https://doi.org/10.1007/s12613-017-1472-8

Lei Zhou, Yan-fang Zhang, Pan Yi, Ying Wen, Chao-fang Dong, Li-min Meng, and Se-fei Yang, Effects of BN content on the mechanical properties of nanocrystalline 3Y-TZP/Al_2O_3/BN dental ceramics, *Int. J. Miner. Metall. Mater.*, 28(2021), No. 11, pp. 1854-1860. https://doi.org/10.1007/s12613-021-2324-0

IJMMM WeChat

QQ author group

International Journal of Minerals, Metallurgy and Materials
Volume 30, Number 5, May 2023, Page 908
https://doi.org/10.1007/s12613-022-2493-5

Achieving oxidation protection effect for strips hot rolling via Al_2O_3 nanofluid lubrication

Jianlin Sun, Boyuan Huang, Jiaqi He✉, Erchao Meng, and Qianhao Chang

School of Materials Science and Engineering, University of Science and Technology Beijing, Beijing 100083, China
(Received: 14 January 2022; revised: 28 March 2022; accepted: 6 April 2022)

Abstract: It was discovered the application of Al_2O_3 nanofluid as lubricant for steel hot rolling could synchronously achieve oxidation protection of strips surface. The underlying mechanism was investigated through hot rolling tests and molecular dynamics (MD) simulations. The employment of Al_2O_3 nanoparticles contributed to significant enhancement in the lubrication performance of lubricant. The rolled strip exhibited the best surface topography that the roughness reached lowest with the sparsest surface defects. Besides, the oxide scale generated on steel surface was also thinner, and the ratio of Fe_2O_3 among various iron oxides became lower. It was revealed the above oxidation protection effect of Al_2O_3 nanofluid was attributed to the deposition of nanoparticles on metal surface during hot rolling. A protective layer in the thickness of about 193 nm was formed to prevent the direct contact between steel matrix and atmosphere, which was mainly composed of Al_2O_3 and sintered organic molecules. MD simulations confirmed the diffusion of O_2 and H_2O could be blocked by the Al_2O_3 layer through physical absorption and penetration barrier effect.

Keywords: hot rolling; nanofluid; lubricant; oxidation protection; molecular dynamics

1. Introduction

As one of the most important manufacturing processes in the steel forming industry, hot rolling is deployed to obtain the specified dimensions, surface quality, and mechanical properties [1]. Friction and wear are inevitable problems during hot rolling process, resulting in about 30% more energy consumption and material loss [2]. Meanwhile, the surface oxidation of steel under the high-temperature condition of hot rolling decreases productivity seriously. And the indentation of oxide scale into steel matrix can also lead to surface defects and increase the difficulty of subsequent pickling and downstream processing [3]. Accordingly, the application of appropriate lubricants is crucial, such as the rolling oil and emulsion. With the development of nanotechnology over the past decades, nanofluids with excellent thermal conductivity and lubrication performance have attracted increasing attention in the field of hot rolling lubrication [4–5]. In particular, water-based nanofluids usually possess the better colling ability and lower pollution compared to traditional oil-based lubricants, which are of great research value and application prospect for developing novel hot rolling lubricants.

As for the lubrication mechanisms of nanoparticles, related scholars have conducted lots of investigations. The proposed lubrication mechanisms can be summarized as the rolling effect [6], polishing effect [5,7], interlayer sliding effect [2,8], and mending effect [9]. Besides, due to the ultra-high surface energy of nanoparticles, they are easy to deposit and absorb on the metal surface during friction process, thus forming a protective tribofilm. Roy *et al.* [10] studied the performance of CuO and WC nanoparticles in Polyalphaolefin under boundary lubrication conditions. CuO nanoparticles could repair surface defects while WC nanoparticles could form a tribofilm on the friction surface. Wang *et al.* [11] prepared triethanolamine functionalized graphene oxide (TEA-GO) for steel cold rolling. Results showed that an adsorption film was generated on the roll and steel strips by TEA-GO nanofluid to protect the surface from severe wear. Jin *et al.* [12] studied the lubrication properties of Mn_3O_4/graphene nanocomposites in grease. Most of the contact surface was covered by the tribofilm, meanwhile the island effect of graphene further improved the tribofilm strength. Hence, the application of nanofluids for steel hot rolling lubrication has significant research value. It is known that spherical Al_2O_3 nanoparticles have high hardness and good thermal stability. After adding nano-Al_2O_3 to lubricants, their bearing capacity and stability of fluids can be assured. Although Al_2O_3 nanoparticles have been employed for steel cold rolling and cutting lubrication, there is little research on the application of nano-Al_2O_3 for hot rolling lubrication. Our previous studies [13–14] have reported the lubrication performance of Al_2O_3 nanofluid, but the route that uses Al_2O_3 nanofluid to achieve oxidation protection effect during steel hot rolling lubrication is original and cutting edge. Hence, Al_2O_3 nanofluid was

✉ Corresponding author: Jiaqi He E-mail: ustbhjq@163.com

employed for steel hot rolling in this investigation.

In addition to being used as lubricant additives, nanoparticles have also been widely applied in metal anti-corrosion coatings, such as TiO_2 [15], SiO_2 [16], Al_2O_3 [17], and graphene oxide [18]. Related studies have confirmed that nanoparticles exhibited superior penetration barrier effect to ions and molecules. For instance, Aliyu *et al.* [19] synthesized graphene nanoparticles reinforced coatings for Al alloy and found that the incorporation of graphene improved the barrier and corrosion protection behavior of coatings. Yu *et al.* [20] prepared graphene oxide–alumina hybrid nanoparticles and then they were applied in epoxy coatings. The hybrid nanoparticles exhibited significant effect in enhancing the corrosion resistance of epoxy coatings, which was attributed to the excellent plugging micro-pore property of nanoparticles. Ding *et al.* [21] applied ZrO_2 and MoS_2 nanoparticles in corrosion-resistant coatings for titanium alloy. It was found that nanoparticles blocked the gaps between coatings to further prevent direct contact between the metal surface and corrosive ions. Based on the application of nanoparticles in the field of corrosion-resistant coatings, combined with their adsorption and film-forming capacities, it is feasible to use nanoparticles in steel hot rolling to restrain the high-temperature oxidation of the metal surface. Besides, Al_2O_3 has been commonly used as anti-corrosion and thermal insulation material. Therefore, we considered the creative application of Al_2O_3 nanoparticles for strip hot rolling lubrication to achieve surface oxidation inhibition under the guarantee of lubrication performance. More recently, the molecular dynamics (MD) method has become a crucial auxiliary means to predict or reproduce the behavior of nanofluids during friction and lubrication process [22–23]. Therefore, MD simulation was also adopted in the present study to reveal the oxidation protection mechanism of nanoparticles for steel strips during hot rolling from the atomic scale.

In this study, water-based Al_2O_3 nanofluid was first prepared as lubricant for steel hot rolling to achieve oxidation protection effect synchronously. Next, hot rolling tests of steel strips were carried out to the lubrication performance of Al_2O_3 nanofluid. Afterward, the effects of nanofluid on the hot rolling force, rolled surface topography, and oxide scale structure were characterized. Finally, MD simulations were conducted to explore the effect of Al_2O_3 nanoparticles on the diffusion behavior of oxidizing atmosphere molecules (O_2 and H_2O) to reveal the corresponding mechanism.

2. Experimental

2.1. Materials and preparation of lubricants

Al_2O_3 nanoparticles (α-phase, 30 nm), sodium dodecylbenzene sulfonate (SDBS, analytical reagent), and sodium hexametaphosphate (SHMP, chemically pure) were provided by Macklin Biochemical, Co., Ltd., China. Triethanolamine (TEA, >99%), glycerol (>98%), and carboxymethylcellulose (CMC, analytical reagent) were obtained from the Sinopharm Chemical Reagent, Co., Ltd., China. All materials and reagents in this study were used as received without further purification.

The preparation process of Al_2O_3 nanofluid was as follows. Firstly, Al_2O_3 nanoparticles were added to the deionized water under continuous stir. Next, TEA and glycerol were added to adjust viscosity and improve the lubrication performance of the fluid. Then, CMC, SDBS, and SHMP were added gradually as surfactants and dispersants. Finally, after sufficient stir and ultrasonic treatment, Al_2O_3 nanofluid was obtained. The concentration of Al_2O_3 nanoparticles in nanofluid was 5wt%. Besides, the base-fluid without nanoparticles was also prepared as the control group, and other substances in the base-fluid were identical to these Al_2O_3 nanofluid.

2.2. Hot rolling tests

A ϕ320 mm × 200 mm two-high rolling mill was employed to study the rolled surface quality and oxidation behavior of steel strips under different lubrication conditions, as shown in Fig. 1. The steel strips for hot rolling were made from E235B steel (ISO 630-2011) with an initial dimension of 70 mm × 50 mm × 30 mm and chemical compositions were listed in Table 1. The strips surface was polished to surface roughness (R_a) of 0.5 μm and cleaned with acetone thoroughly. The samples were heated to 1200°C in an argon-atmosphere furnace and held for 1.5 h to ensure they were heated fully. The initial rolling temperature was controlled at (1050 ± 10)°C using a temperature measuring gun. The nominal rolling speed was 0.5 $m \cdot s^{-1}$, and the samples were rolled from 30 to 4 mm in five passes. The hot rolling tests were conducted without lubrication, with base-fluid or with Al_2O_3 nanofluid, respectively. The base-fluid or Al_2O_3 nanofluid was applied abundantly during the processes as lubricant. Subsequently, the rolled strips were cooled to room temper-

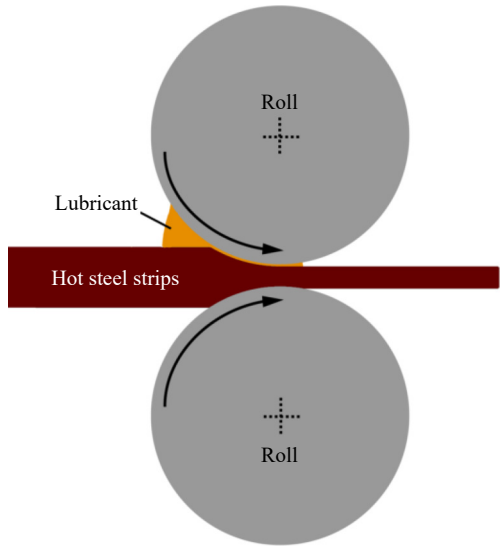

Fig. 1. Schematic diagram of the two-high hot rolling mill.

Table 1. Chemical compositions of E235B steel strips wt%

C	Mn	Si	P	S	Cr	Fe
0.17	1.47	0.30	<0.042	<0.039	0.03	Balance

ature. All tests were repeated three times to avoid contingency.

2.3. Characterization methods

The surface topography, profile curve, and roughness of rolled strips surface were acquired using a laser scanning confocal microscope (LSCM, Olympus LEXTOLS 4100, Japan). A scanning electron microscope (SEM, ZEISS Gemini 500, Germany) equipped with an energy dispersive spectrometer (EDS) was employed to characterize the cross-section of strips to get the oxide layer structure, thickness, and element distribution. To further analyze the phase composition of the oxide layer, X-ray diffraction (XRD, Rigaku Ultima IV, Japan) was performed at 30 kV, 150 mA with Cu-K_α radiation in the 2θ range of 20°–80°.

2.4. MD simulation details

To determine the oxidation inhibition mechanism of Al_2O_3 nanofluid during strips hot rolling, MD simulation was conducted to study the diffusion behavior of oxidizing atmosphere molecules (O_2 and H_2O) on the steel surface. As shown in Fig. 2, the models without Al_2O_3 (001) layer (Fig. 2(a)) and containing Al_2O_3 (001) layer (Fig. 2(b)) on Fe (110) slab were built to simulate the hot rolling process without and with Al_2O_3 nanofluid, which was marked as Model-F and Model-FA, respectively. Each model contained 50 O_2 and 50 H_2O molecules. The total size of MD models was 8 nm × 5 nm × 6 nm and the size of Al_2O_3 layer in Fig. 2(b) was 8 nm × 5 nm × 0.65 nm. The interatomic and van der Waals' interactions between atoms were modified by the Universal forcefield, which is suitable for obtaining the diffusion and absorption properties of molecules [24]. The study focuses on the behavior of oxidizing atmosphere molecules, hence the Al_2O_3 layer and Fe slab were set as rigid layers, while the O_2 and H_2O molecules could move freely.

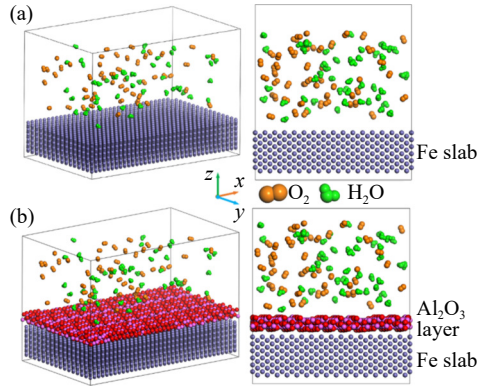

Fig. 2. MD simulation model for the behavior of O_2 and H_2O molecules on the Fe surface (a) without protection (Model-F) and (b) with Al_2O_3 layer (Model-FA).

After the above model setup stage, dynamics simulation stage was performed. Firstly, the pressure P_0 = 100 MPa was applied along the negative z-direction to simulate the pressure during the actual hot rolling process. Meanwhile, the temperature was maintained at 900, 1000, 1100, 1200, or 1300°C by the Nose–Hoover thermostat [25]. Then the simulation system was relaxed adequately for 200 ps to reach the equilibrium state under the canonical (NVT) ensemble. Secondly, the atmosphere molecules were diffused freely at the set temperature and pressure for 1000 ps and the time step was 1 fs. The motion trajectory and velocity of molecules were recorded and exported every 10 ps. The mean square displacement (MSD) and diffusion coefficient (D) of molecules were obtained by Eqs. (1) and (2):

$$\mathrm{MSD}(t) = \frac{1}{N}\left\langle \sum_{i=1}^{N} |r_i(t) - r_i(0)|^2 \right\rangle \tag{1}$$

$$D = \frac{1}{6}\lim_{t\to\infty}\left(\frac{\mathrm{d}}{\mathrm{d}t}\mathrm{MSD}(t)\right) \tag{2}$$

where N is the total number of atoms, $r_i(t)$ is the position of atom i at time t, and $r_i(0)$ is the initial position of atom.

3. Results and discussion

3.1. Hot rolling lubrication performance

During hot rolling processes, sufficient lubricants were applied on the strip surface for every pass, as shown in Fig. 3(a). Photos of the rolled steel strip under different lubricating conditions were presented in Fig. 3(b). It could be found that all the samples exhibited normal strip shape, but there were significant differences in their surface finish. Compared with the sample under no lubrication and base-fluid lubrication, the rolled strip surface lubricated with Al_2O_3 nanofluid was brighter with smoother surface topography. At the same time, with the improvement of lubrication effect, the brown oxides on the hot-rolled surface also gradually reduced, namely the typical high-valance iron oxide Fe_2O_3.

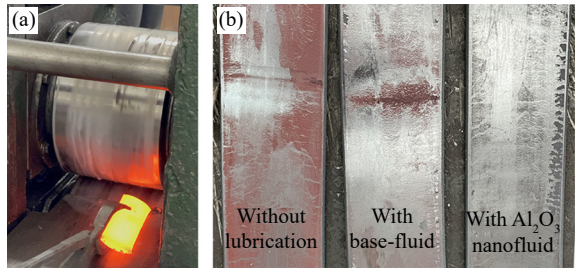

Fig. 3. Photos of (a) hot rolling process and (b) rolled steel strips.

The variation of hot rolling force for each pass under different lubricating conditions was shown in Fig. 4. And the finish rolling thickness of the rolled strip without lubrication, with base-fluid, and with Al_2O_3 nanofluid was 4.51, 4.43, and 4.24 mm, respectively. According to Stone's formula [4,26] shown in Eqs. (3) and (4), lower rolling force F and closer finish thickness $h_{\min}$ to the final rolling gap setting (4 mm) usually indicates lower friction coefficient μ, which reflects better lubrication performance:

$$\frac{F}{S} = \frac{(\mathrm{e}^{\mu l/h} - 1)\sigma}{\mu l/h} \tag{3}$$

$$h_{\min} = 3.58\frac{\mu D(K-q)}{E} \tag{4}$$

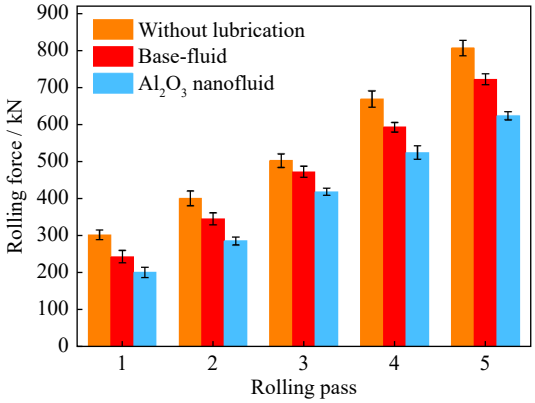

Fig. 4. Hot rolling force of the strips under different lubricating conditions.

where S, l, and h are the average area, arc length, and thickness of steel strip in the contact region, respectively. And the tension of rolling q, diameter D, and elasticity modulus E of the working roll, deformation resistance σ, and rolling stiffness coefficient K are related to the rolling mill and steel strip. Hence, the application of Al_2O_3 nanofluid contributed to the lowest average rolling force (409.0 kN), which was decreased by about 23.5% and 13.6% compared to that rolled without lubrication and with base-fluid, respectively. Meanwhile, the finish rolling thickness was the closest to the preset state in this case.

Surface topography micrographs and the corresponding surface profile curves along y = 1280 μm of the rolled strips under different lubricating conditions were shown in Fig. 5. Parameters for evaluating the surface roughness including the average centerline value (R_a), the maximum peak height (R_p), and the maximum valley depth (R_v) of the profile were also measured and presented. For the hot-rolled strip surface without lubrication, as shown in Fig. 5(a), large areas of dark regions and furrows could be observed on the surface. It could be seen from the 3D topography that these dark regions were mostly lower (appears blue in the 3D graph) than other places, which was the typical feature of severe adhesive wear that the metal on the strip surface was torn off and transferred to the working roll. And the furrows along the rolling direction were caused by the abrasive wear, which was mainly attributed to the scratch of asperities and wear particles to the friction surfaces. Meanwhile, the ductility and thermal expansion property of the oxide scale formed during hot rolling were quite different from those of the steel matrix [27]. Then under high pressure, these oxides were easily crushed and thus impacting the surface quality. As shown in Fig. 5(b), when the base-fluid was applied as lubricant for the hot rolling process, dark regions on the rolled surface became fewer that the adhesive wear was alleviated due to the anti-wear and friction-reducing effect of base-fluid. The reduce of R_p and R_v value also indicated the rolled surface was more uniform with lower asperities and shallower grooves. Further, as can be seen from Fig. 5(c), when Al_2O_3 nanofluid with better lubrication performance was employed, the smoothest strip surface was obtained that the R_a value was re-

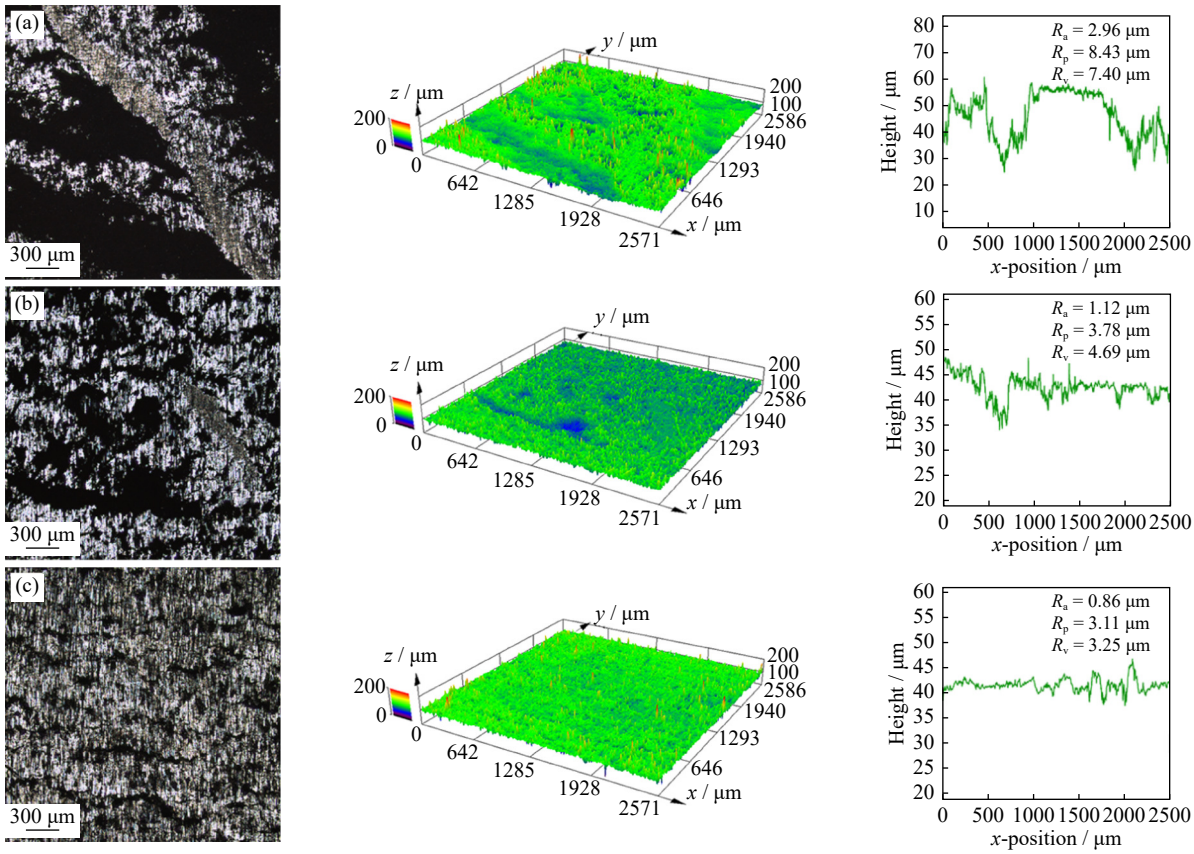

Fig. 5. Surface topography micrographs and corresponding surface profile curves for the rolled strips (a) without lubrication, (b) with base-fluid, and (c) with Al_2O_3 nanofluid.

duced from 1.12 to 0.86 μm. There were few surface defects on surface such as scratches, pits, and especially metal adhesions almost disappeared. In summary, the application of Al_2O_3 nanofluid as lubricant for steel hot rolling could alleviate the rolling force as well as the friction between strip and working roll, which could improve the surface quality of rolled products, reduce material loss and energy consumption.

3.2. Analysis of oxide scale on the rolled surface

The SEM images of the cross-section micrographs for the hot-rolled strips under different lubricating conditions were shown in Fig. 6. The corresponding EDS line scan results along the red arrows in SEM images were also listed. The oxide scale thickness could be obtained by analyzing the variation of Fe and O element content. It can be seen from Fig. 6(a) that the oxide scale formed on the strip surface without any lubrication was quite thick. The average thickness was about 78.8 μm and there were several cracks and cavities in the oxide layer. The interface between the oxide scale and steel matrix was uneven with several zigzags. While with the application of base-fluid, the oxide scale thickness became lower to about 60.4 μm on average with a few voids and cracks. The interface was slightly smoother and the zigzags became fewer. When the steel strip was lubricated by Al_2O_3 nanofluid during hot rolling, the oxide scale generated on the surface was the thinnest (about 39.5 μm), indicating the lowest degree of metal oxidation. Furthermore, Al elements were detected at the interface between oxide scale and resin, so it can be speculated that Al_2O_3 nanoparticles had been deposited on the surface and a layer might be formed.

The XRD patterns of oxide scale on the rolled surface under different lubricating conditions were shown in Fig. 7. The peaks of Fe_2O_3 (JCPDS card No. 99-0060), Fe_3O_4 (JCPDS card No. 99-0073), and FeO (JCPDS card No. 75-1550) were

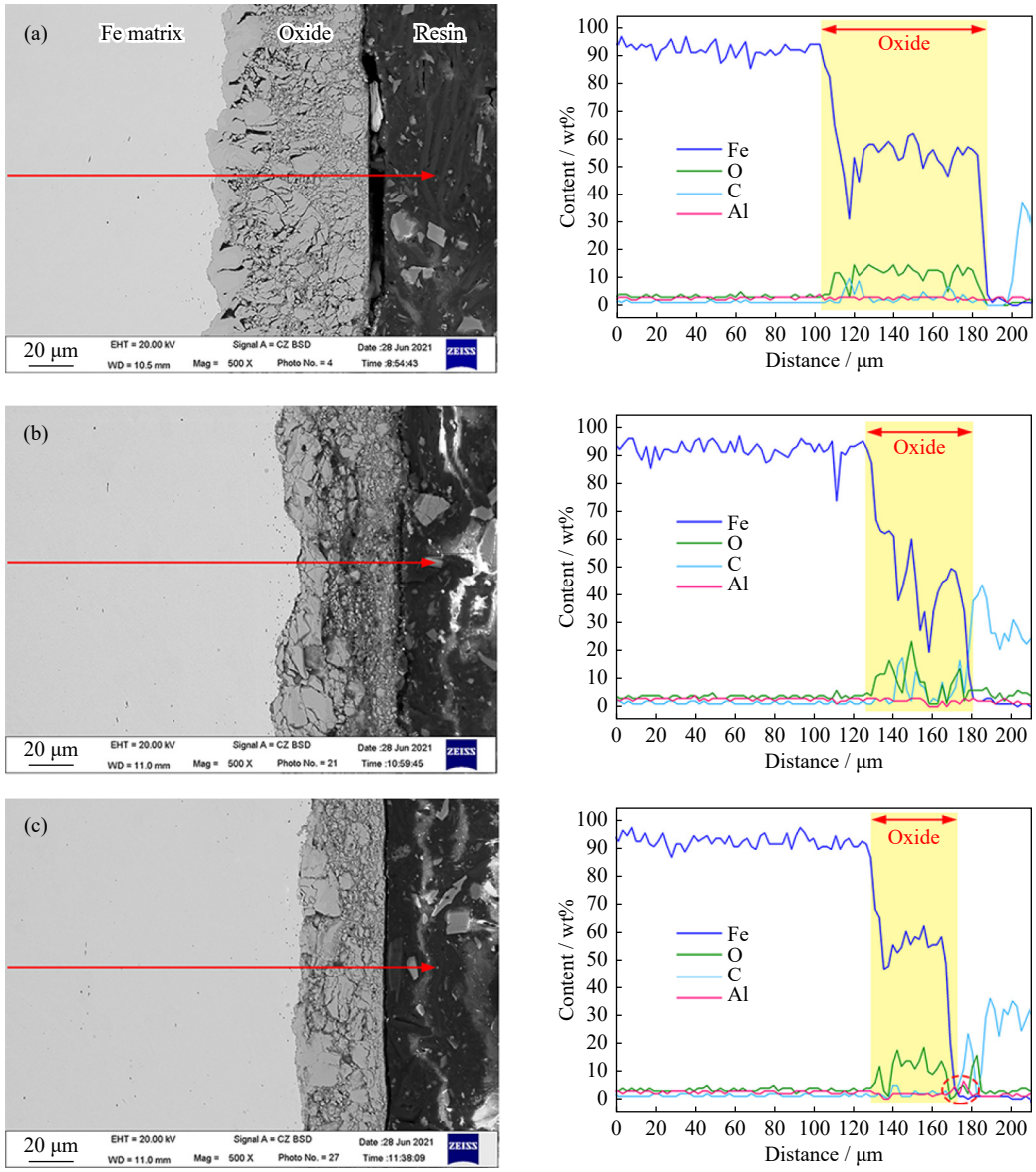

Fig. 6. SEM and the corresponding EDS result for the cross-section structure of the rolled strips (a) without lubrication, (b) with base-fluid, and (c) with Al_2O_3 nanofluid.

highlighted in the figure. It can be seen from Fig. 7(a) and (b) that the oxide scale on the rolled surface without lubrication and lubricated with base-fluid were mainly composed of Fe_2O_3 and Fe_3O_4. After the application of base-fluid, the characteristic peaks of Fe_3O_4 became slightly more pronounced. As shown in Fig. 7(c), the employment of Al_2O_3 nanoparticles made this phenomenon more remarkable that the peaks of Fe_2O_3 significantly weakened, meanwhile the peaks at 42.1° and 61.1° indicated the presence of FeO. Hence, it can be inferred that due to the excellent lubrication performance of Al_2O_3 nanofluid, the oxide scale formed on steel surface was denser. And the superior thermal conductivity of nanofluid further promoted the cooling of high-temperature steel strips during hot rolling [28]. The oxidation time of metal surface was shortened and then the oxide scale was thinned.

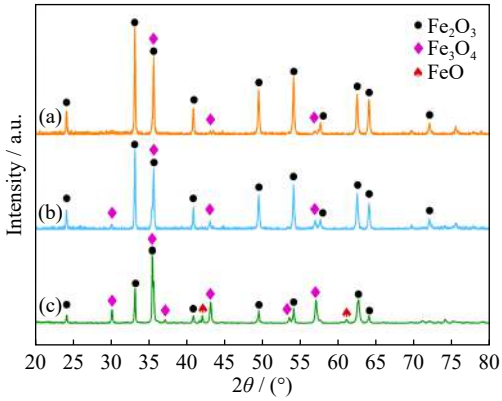

Fig. 7. XRD analysis result of the oxide scale on the rolled surface (a) without lubrication, (b) with base-fluid, and (c) with Al_2O_3 nanofluid.

To further clarify the role of Al_2O_3 nanoparticles for the oxidation of steel surface, the outmost area of the rolled surface was characterized by the scanning-transmission electron microscopy (STEM) mode of TEM. As shown in Fig. 8, a distinct alumina layer with an average thickness of about 193 nm appeared outside the oxide scale. The structure of this layer was relatively compact. In addition to Al element, significant amounts of C elements were found in the layer. Hence, it can be confirmed that Al_2O_3 nanoparticles and these organic molecules in nanofluid could indeed be deposited and absorbed on the steel surface during the hot rolling process. The density and stability of this protective layer could

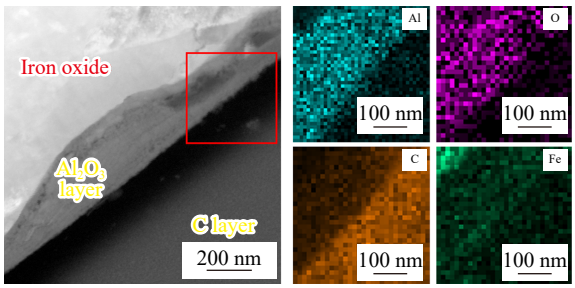

Fig. 8. STEM image and corresponding EDS map results of the outmost area of the rolled surface.

inhibit the steel surface from direct contact with oxidation atmosphere to achieve the anti-oxidation function.

3.3. MD simulation on the diffusion of oxidation molecules

In this section, the effect of Al_2O_3 layer on metal oxidation would be discussed in detail according to MD simulation results. The variation of MSD along *z*-direction for O_2 and H_2O molecules in different models under every simulation temperature is shown in Fig. 9. The corresponding diffusion coefficient *D* was calculated and listed in Table 2. Generally, the lower MSD and *D* indicate the diffusion of molecules is inhibited. It can be seen that the existence of Al_2O_3 layer on the Fe surface has obvious inhibitory effect on the diffusion of two kinds of oxidizing atmosphere molecules to Fe slab. By analyzing the MSD in the final state (1000 ps), the diffusion inhibitory effect of O_2 at 1300°C was about 20.7%, and it was more significant for H_2O molecules. At 1300°C, the MSD of H_2O at the final state decreased from 2.38×10^4 to 1.34×10^4 nm^2 that the diffusion inhibition efficiency reached 43.7%. The van der Waals' interaction volume (2.06×10^{-2} nm^3) and surface area (1.304 nm^2) of H_2O were calculated to be lower than the interaction volume (2.45×10^{-2} nm^3) and surface area (1.430 nm^2) of O_2 molecule. Therefore, the free volume fraction of H_2O was larger, thus its pore volume utilization rate of the Al_2O_3 layer was also higher than O_2 [29], then the Al_2O_3 layer exhibited stronger obstruction ability to the diffusion of H_2O than O_2 molecules. As a result, the decrease of the MSD value of H_2O molecules was more obvious.

With the increase of temperature, the diffusion coefficient *D* of the two kinds of molecules showed an upward trend, indicating that the thermal motion of molecules became more intense. Generally, the variation of diffusion coefficient *D* with temperature reflects the kinetic law of chemical reaction [30]. To evaluate the tendency of the oxidation reaction of different samples, the activation energy of oxidation reaction was obtained by the Arrhenius formula [31], as shown in Eq. (5):

$$D = D_o \exp\left(-\frac{Q_o}{RT}\right) \tag{5}$$

where Q_o is the activation energy of oxidation ($J \cdot mol^{-1}$), D_o is the Arrhenius constant, *R* is the ideal gas constant (8.314 $J \cdot mol^{-1} \cdot K^{-1}$), and *T* is the absolute temperature with the unit K. By fitting these *D* values according to Eq. (5), the oxidation kinetics equation and activation energy could obtain. When the surface of steel strips was not protected by the Al_2O_3 layer: *D* (O_2 in Model-F) = $1.55 \times 10^{-4} \cdot \exp(-5608.3/T)$, *D* ($H_2O$ in Model-F) = $1.90 \times 10^{-4} \cdot \exp(-5815.8/T)$, Q_o (O_2 in Model-F) = 46.6 $kJ \cdot mol^{-1}$, and Q_o (H_2O in Model-F) = 48.4 $kJ \cdot mol^{-1}$. When the Fe surface was coated with Al_2O_3 layer: *D* (O_2 in Model-FA) = $0.92 \times 10^{-4} \cdot \exp(-5429.4/T)$, *D* ($H_2O$ in Model-FA) = $0.30 \times 10^{-4} \cdot \exp(-3667.5/T)$, Q_o (O_2 in Model-FA) = 45.1 $kJ \cdot mol^{-1}$, Q_o (H_2O in Model-FA) = 30.5 $kJ \cdot mol^{-1}$. From the oxidation kinetics above, the lower Arrhenius constant D_0 for the mo-

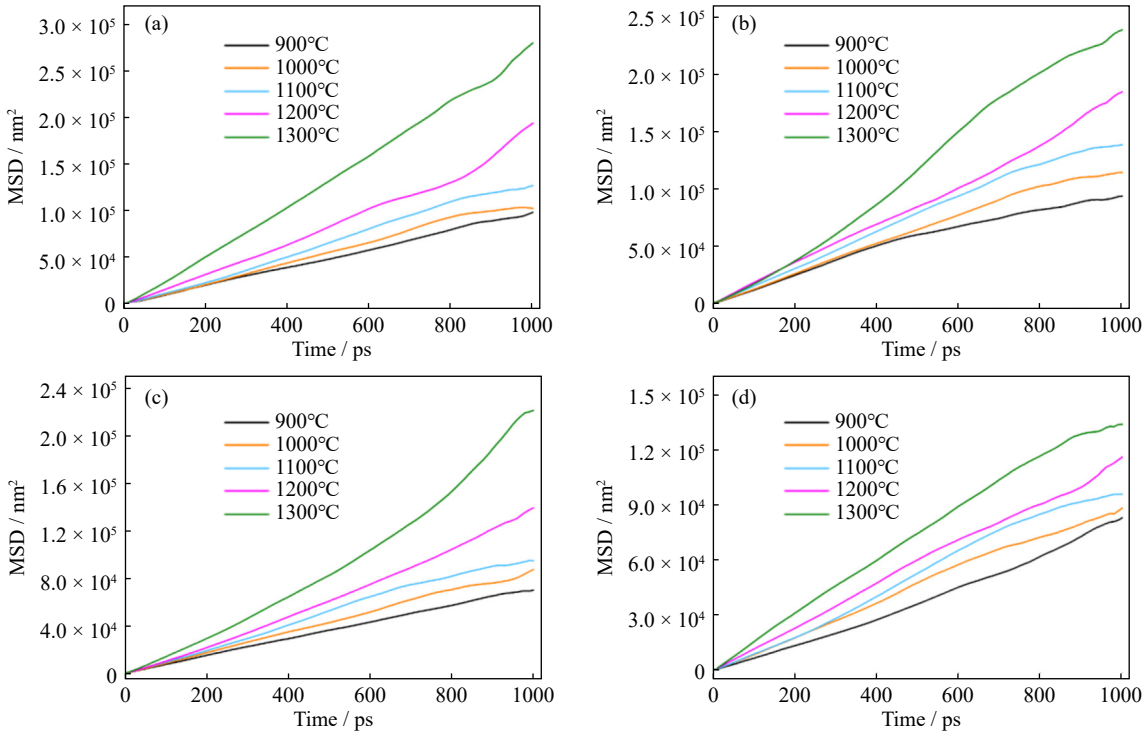

Fig. 9. Variation of MSD of atmosphere molecules at different temperature: (a) O_2 in Model-F, (b) H_2O in Model-F, (c) O_2 in Model-FA, and (d) H_2O in Model-FA.

Table 2. Diffusion coefficient D of O_2 and H_2O molecules in different models 10^{-6} m^2·s^{-1}

Molecule	Condition	900°C	1000°C	1100°C	1200°C	1300°C
O_2	Without Al_2O_3	1.545	1.955	2.468	3.103	4.646
	With Al_2O_3	1.168	1.482	1.893	2.535	3.337
H_2O	Without Al_2O_3	1.516	2.117	2.630	3.283	4.986
	With Al_2O_3	1.378	1.639	1.981	2.417	2.934

lecules in Model-FA confirmed that Al_2O_3 layer inhibited the diffusion of O_2 and H_2O, and thus reduced the rate of oxidation reaction. More importantly, the oxidation activation energy Q_o for both O_2 and H_2O also decreased to a certain extent, indicating that the increasing trend of diffusion rate of molecules to the metal surface became moderate with the rise of temperature [32]. The mechanism of this phenomenon will be revealed by the following analysis on the position, relative concentration distribution, and adsorption behavior of molecules in different models.

The snapshots of the MD simulation models in the final state (1000 ps) at 1300°C are shown in Fig. 10, and the relative concentration distribution curves of O_2 and H_2O along z-direction at 900 and 1300°C are presented. As shown in Fig. 10(a), when the Fe slab was exposed to the oxidizing atmosphere directly, both the concentrations of O_2 and H_2O molecules on Fe surface were relatively high, and the change of temperature had no obvious effect on their distribution. When the strips surface was protected by Al_2O_3 layer, as shown in Fig. 10(b), many atmosphere molecules gathered

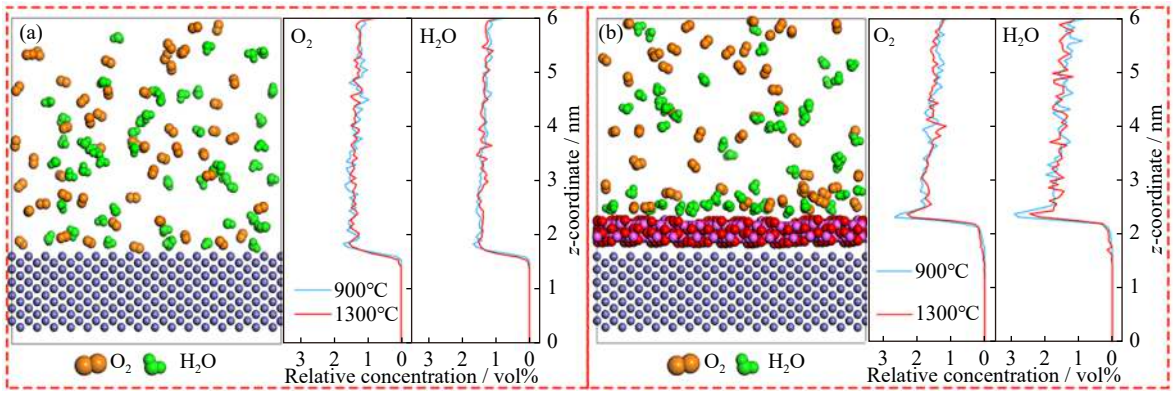

Fig. 10. Distribution and relative concentration profile of O_2 and H_2O molecules for the system (a) without Al_2O_3 layer and (b) with Al_2O_3 layer.

on the upper surface of Al_2O_3 layer. The corresponding concentrations were close to 3vol%, which was higher than other positions distinctly. At the same time, very few molecules have diffused to the Fe surface. Since the simulation method adopted in this study was the classical molecular dynamics, only the non-bonding interactions between atoms and molecules can be obtained, so the chemical reaction processes including electron transfer and covalent bond formation/breaking were not available directly [33]. Therefore, considering the extremely high chemical reaction inertia of Al_2O_3, the accumulation of molecules on the upper surface of Al_2O_3 layer was mainly due to the physical adsorption and penetration barrier effect of Al_2O_3 layer. With the increase of temperature, the concentration of adsorbed molecules decreased slightly. The physical adsorption strength weakened, which was consistent with the Langmuir adsorption model [34]. The physical adsorption and penetration barrier effect reduced the diffusion coefficient of O_2 and H_2O molecules effectively, and the certain adsorption strength of molecules on Al_2O_3 layer also reduced the sensitivity of diffusion coefficient to the temperature rise.

However, under the forcefield of classical molecular dynamics, there was no similar aggregation of molecules on the Fe surface in Fig. 10(a), indicating that the interaction between O_2/H_2O molecules and steel strips surface tended to be chemical reactions rather than physical processes. At this time, the diffusion coefficient was also higher, which increased the frequency and amplitude of collisions between O_2/H_2O molecules and Fe atoms on surface, thus promoting the occurrence of oxidation reaction and formation of the oxide layer. The adsorption energy E_{ads} of a single O_2 or H_2O molecule on Fe or Al_2O_3 surface was calculated. The adsorption energy of O_2 or H_2O on Fe surface was −125.4 and −133.7 kJ·mol^{-1}, respectively, while this value was −27.5 and −32.4 kJ·mol^{-1} on the Al_2O_3 surface, respectively. All adsorption energy values were negative, which showed that the atmosphere molecules had obvious attraction effect on the two solid surfaces [35]. The absolute values of E_{ads} for molecules on the Al_2O_3 surface were both lower than 40 kJ·mol^{-1}, whereas those on the Fe surface were higher and far greater than 40 kJ·mol^{-1}. Hence, it could be confirmed that physical adsorption was the main interaction between O_2/H_2O molecules and the protective Al_2O_3 layer, while chemical adsorption was the typical interaction of them on the more active Fe surface. This result further proved that O_2 and H_2O molecules were easy to oxidize with the high-temperature Fe surface, and there was only physical interaction with chemically inert Al_2O_3 layer, which was consistent with the MD simulation results above.

3.4. Discussion on the oxidation protection mechanism

Based on the results and analysis above, the proposed oxidation protection mechanism of Al_2O_3 nanofluid was summarized and discussed. During the hot rolling process, steel strips were heated to high temperature and exposed to the air atmosphere completely. Air molecules including O_2 and H_2O collided with metal surface intensely and then chemical reactions occurred to form iron oxides. When nanofluid was applied as hot rolling lubricant, Al_2O_3 nanoparticles spread out quickly on the steel surface. Due to the deposition and absorption of Al_2O_3 nanoparticles and other substances from the nanofluid, a protective Al_2O_3 layer would be formed. On the one hand, this layer could act as the most direct barrier preventing the steel strips from contacting oxidizing molecules. On the other hand, these atmosphere molecules could be physically absorbed by Al_2O_3. Then fewer molecules were able to cross the protective layer and reach the pre-generated oxide layer or even the matrix-oxide layer interface. Afterward, the chemical reactions shown in Eqs. (6) to (8) at the interface were inhibited:

$$2Fe + O_2 = 2FeO \tag{6}$$

$$5FeO + O_2 = Fe_3O_4 + Fe_2O_3 \tag{7}$$

$$3Fe + 4H_2O(g) = Fe_3O_4 + 4H_2 \tag{8}$$

As a result, the oxide layer generated on the rolled strips surface became thinner significantly. Oxidation protection was hereby realized meanwhile contributing to the reduction in material loss and energy consumption.

4. Conclusion

In the present study, Al_2O_3 nanofluid was prepared as lubricant for steel strips hot rolling to induce oxidation protection effect synchronously. The effect of Al_2O_3 nanoparticles on oxide scale evolution of the rolled surface was investigated through experiments and MD simulation. Results showed that Al_2O_3 nanofluid exhibited excellent lubrication performance that contributed to about 13.6% reduction in average hot rolling force compared with the base-fluid, and the finish rolling thickness was also the closest to the pre-set value. The rolled steel surface had the optimal quality with the lowest roughness and fewest surface defects. By analyzing the oxide scale structure and composition formed on the rolled surface, the thickness was about 34.6% thinner and denser with lower proportion of high-valance iron oxide (Fe_2O_3). More importantly, Al_2O_3 nanoparticles were observed to be deposited at the contact interface. The protective Al_2O_3 layer in a thickness of about 193 nm formed on rolled surface played a vital role in inhibiting the continuous oxidation of high-temperature steel strips. Besides, MD simulation results confirmed that the Al_2O_3 layer could inhibit the diffusion of O_2 and H_2O molecules mainly through physical absorption and penetration barrier effect. The oxide reaction at hot steel strip surface was thus suppressed and the thickness of oxide scale was reduced. This study provides a new route for solving the surface oxidation problem of steel strips during hot rolling process.

Acknowledgements

This work was financially supported by the National Natural Science Foundation of China (No. 51874036) and Na-

tional Key Research and Development Program of China (No. 2021YFB3701305).

Conflict of Interest

The authors declare no conflict of interest.

References

[1] L. Wang, A.K. Tieu, H.T. Zhu, G.Y. Deng, S.G. Cui, and Q. Zhu, A study of water-based lubricant with a mixture of polyphosphate and nano-TiO_2 as additives for hot rolling process, *Wear*, 477(2021), art. No. 203895.

[2] A.I. Khdair and A. Ibrahim, Effect of graphene addition on the physicomechanical and tribological properties of Cu nanocomposites, *Int. J. Miner. Metall. Mater.*, 29(2022), No. 1, p. 161.

[3] X.L. Yu, Z.Y. Jiang, J.W. Zhao, *et al*., The role of oxide-scale microtexture on tribological behaviour in the nanoparticle lubrication of hot rolling, *Tribol. Int.*, 93(2016), p. 190.

[4] S. Xiong, D. Liang, H. Wu, W. Lin, J.S. Chen, and B.S. Zhang, Preparation, characterization, tribological and lubrication performances of Eu doped $CaWO_4$ nanoparticle as anti-wear additive in water-soluble fluid for steel strip during hot rolling, *Appl. Surf. Sci.*, 539(2021), art. No. 148090.

[5] Y.Y. Bao, J.L. Sun, and L.H. Kong, Effects of nano-SiO_2 as water-based lubricant additive on surface qualities of strips after hot rolling, *Tribol. Int.*, 114(2017), p. 257.

[6] Y.N. Wang, Z.P. Wan, L.S. Lu, Z.H. Zhang, and Y. Tang, Friction and wear mechanisms of castor oil with addition of hexagonal boron nitride nanoparticles, *Tribol. Int.*, 124(2018), p. 10.

[7] N.G. Demas, R.A. Erck, C. Lorenzo-Martin, O.O. Ajayi, and G.R. Fenske, Experimental evaluation of oxide nanoparticles as friction and wear improvement additives in motor oil, *J. Nanomater.*, 2017(2017), art. No. 8425782.

[8] L. Xu, T.B. Ma, Y.Z. Hu, and H. Wang, Molecular dynamics simulation of the interlayer sliding behavior in few-layer graphene, *Carbon*, 50(2012), No. 3, p. 1025.

[9] K. Li, X. Zhang, C. Du, *et al*., Friction reduction and viscosity modification of cellulose nanocrystals as biolubricant additives in polyalphaolefin oil, *Carbohydr. Polym.*, 220(2019), p. 228.

[10] S. Roy, Y. Jazaa, and S. Sundararajan, Investigating the micropitting and wear performance of copper oxide and tungsten carbide nanofluids under boundary lubrication, *Wear*, 428-429(2019), p. 55.

[11] C.L. Wang, J.L. Sun, C.L. Ge, and P. Wu, Enhanced lubrication performance of triethanolamine functionalized reduced graphene oxide on the cold-rolled surface of strips, *Surf. Interface Anal.*, 53(2021), No. 9, p. 762.

[12] B. Jin, G.Y. Chen, J. Zhao, Y.Y. He, Y.Y. Huang, and J.B. Luo, Improvement of the lubrication properties of grease with Mn_3O_4/graphene (Mn_3O_4#G) nanocomposite additive, *Friction*, 9(2021), No. 6, p. 1361.

[13] J.Q. He, J.L. Sun, Y.N. Meng, and Y. Pei, Superior lubrication performance of MoS_2–Al_2O_3 composite nanofluid in strips hot rolling, *J. Manuf. Process.*, 57(2020), p. 312.

[14] J.Q. He, J.L. Sun, Y.N. Meng, H.J. Tang, and P. Wu, Improved lubrication performance of MoS_2–Al_2O_3 nanofluid through interfacial tribochemistry, *Colloids Surf. A*, 618(2021), art. No. 126428.

[15] P. Baghery, M. Farzam, A.B. Mousavi, and M. Hosseini, Ni–TiO_2 nanocomposite coating with high resistance to corrosion and wear, *Surf. Coat. Technol.*, 204(2010), No. 23, p. 3804.

[16] A. Kumar and M.K. Meena, Fabrication of durable corrosion-resistant polyurethane/SiO_2 nanoparticle composite coating on aluminium, *Colloid Polym. Sci.*, 299(2021), No. 6, p. 915.

[17] S. Dehgahi, R. Amini, and M. Alizadeh, Microstructure and corrosion resistance of Ni–Al_2O_3–SiC nanocomposite coatings produced by electrodeposition technique, *J. Alloys Compd.*, 692(2017), p. 622.

[18] A.K. Behera, A. Das, S. Das, and A. Mallik, Electrochemically functionalized graphene as an anti-corrosion reinforcement in Cu matrix composite thin films, *Int. J. Miner. Metall. Mater.*, 28(2021), No. 9, p. 1525.

[19] I.K. Aliyu, M.K. A, and A.S. Mohammed, Wear and corrosion resistance performance of UHMWPE/GNPs nanocomposite coatings on AA2028 Al alloys, *Prog. Org. Coat.*, 151(2021), art. No. 106072.

[20] Z.X. Yu, H.H. Di, Y. Ma, *et al*., Fabrication of graphene oxide-alumina hybrids to reinforce the anti-corrosion performance of composite epoxy coatings, *Appl. Surf. Sci.*, 351(2015), p. 986.

[21] X.X. Ding, L. Wu, J. Chen, *et al*., A. Atrens, and F.S. Pan, Enhanced protective nanoparticle-modified MgAl-LDHs coatings on titanium alloy, *Surf. Coat. Technol.*, 404(2020), art. No. 126449.

[22] Y.Y. Tian, H. Feng, J. Li, Q.H. Fang, and L.C. Zhang, Nanoscale sliding friction behavior on Cu/Ag bilayers influenced by water film, *Appl. Surf. Sci.*, 545(2021), art. No. 148957.

[23] L.P. Wu, L.M. Keer, J. Lu, B.Y. Song, and L. Gu, Molecular dynamics simulations of the rheological properties of graphene–PAO nanofluids, *J. Mater. Sci.*, 53(2018), No. 23, p. 15969.

[24] A.K. Rappe, C.J. Casewit, K.S. Colwell, W.A. Goddard III, and W.M. Skiff, UFF, a full periodic table force field for molecular mechanics and molecular dynamics simulations, *J. Am. Chem. Soc.*, 114(1992), No. 25, p. 10024.

[25] D.J. Evans and B.L. Holian, The Nose–Hoover thermostat, *J. Chem. Phys.*, 83(1985), No. 8, p. 4069.

[26] Y.L. Kang and J.L. Sun, *Rolling Engineering*, 2nd ed, Metallurgical Industry Press, Beijing, 2014.

[27] R.P. Matthews, R.D. Knusten, J.E. Westraadt, and T. Couvant, Intergranular oxidation of 316L stainless steel in the PWR primary water environment, *Corros. Sci.*, 125(2017), p. 175.

[28] W.Z. Xia, J.W. Zhao, H. Wu, S.H. Jiao, and Z.Y. Jiang, Effects of oil-in-water based nanolubricant containing TiO_2 nanoparticles on the tribological behaviour of oxidised high-speed steel, *Tribol. Int.*, 110(2017), p. 77.

[29] L. Jia, Y.Y. Zeng, and T. Zhang, Experimental study on pore distribution characters and convert rate of CaO, *J. Therm. Sci.*, 14(2005), No. 1, p. 87.

[30] Z.N. Zhang, N. Kong, H.B. Li, and J. Zhang, The migration and reaction of ions during the oxidation of Fe–Si alloy with 0.5wt% Si at 1000–1200°C, *Mater. Res. Express*, 5(2018), No. 6, art. No. 066506.

[31] N. Birks, G.H. Meier, and F.S. Pettit, *Introduction to the High Temperature Oxidation of Metals*, 2nd ed., Cambridge University Press, Cambridge, 2006.

[32] H.S. Grewal, R.M. Sanjiv, H.S. Arora, *et al*., Activation energy and high temperature oxidation behavior of multi-principal element alloy, *Adv. Eng. Mater.*, 19(2017), No. 11, art. No. 1700182.

[33] M.H. Du and H.P. Cheng, Transparent interface between classical molecular dynamics and first-principles molecular dynamics, *Int. J. Quantum Chem.*, 93(2003), No. 1, p. 1.

[34] A.W. Marczewski, A. Deryło-Marczewska, and A. Słota, Adsorption and desorption kinetics of benzene derivatives on mesoporous carbons, *Adsorption*, 19(2013), No. 2-4, p. 391.

[35] X.Q. Ma, Y.H. Liu, J.L. Chu, *et al*., Removal of zirconium from hydrous titanium dioxide, *Int. J. Miner. Metall. Mater.*, 20(2013), No. 1, p. 1.